SECONDARY EMISSION MONITOR SIMULATION, MEASUREMENTS AND MACHINE LEARNING APPLICATION STUDIES FOR CERN FIXED TARGET BEAMLINES

L. Parsons França[1,2,3,*], F. Roncarolo[1], F. M. Velotti[1], M. Duraffourg[1], C.P. Welsch[2,3],
H. D. Zhang[2,3], E. Kukstas[2,3]
[1]CERN, Geneva, Switzerland
[2]Cockcroft Institute, Daresbury, UK
[3]University of Liverpool, UK

Abstract

The CERN fixed target experimental areas have recently acquired new importance thanks to newly proposed experiments, such as those linked to Physics Beyond Colliders (PBC) activities. Secondary Emission Monitors (SEMs) are the instruments currently used for measuring beam current, position and size in these areas. Guaranteeing their reliability, resistance to radiation and measurement precision is challenging. This paper presents the studies being conducted to understand ageing effects on SEM devices, to calibrate and optimise the SEM design for future use in these beamlines. These include feasibility studies for the application of machine learning techniques, with the objective of expanding the range of tools available for data analysis.

INTRODUCTION

The TT20 beamline at CERN carries the $400\,\mathrm{GeV}/c$ beam from the SPS towards the fixed target experiments in the North Area (Fig. 1). The slow extracted beam is de-bunched[1], with total intensity ranging from a few 10^{11} (during machine setup and development) to a few 10^{13} protons (during physics), diluted along spills lasting between 1 to 5 seconds. The choice of instrumentation for beam position, size and intensity measurements is at the moment restricted to SEMs and scintillating screens [1].

SEM monitors generally consist of metallic wires or thin foils, intercepting the beam. As the beam passes through these surfaces some particles interact, transferring energy to the material [3]. If the electrons in the metal receive enough energy to escape the Fermi level, they are released, in a process known as Secondary Emission (SE), theoretically described by E. J. Sternglass [4].

The number of electrons emitted per incident proton is defined as the Secondary Emission Yield (SEY) and can be written as [5]:

$$SEY = 0.01 L_s \frac{dE}{dx}|_{el} \left[1 + \frac{1}{1 + (5.4 \cdot 10^{-6} E/A_p)} \right]. \quad (1)$$

It depends on the kinetic energy of the projectile (E), the electronic energy loss ($\frac{dE}{dx}|_{el}$), the mass of projectile (A_p) and the characteristic length of diffusion of low energy electrons

---

* luana.parsons.franca@cern.ch
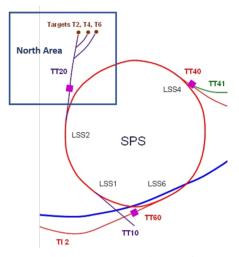[1] The SPS RF is switched off at flat top, before extraction

Figure 1: Schematic representation layout of SPS and North Area beamlines, sourced from [2].

(L_s), given by:

$$L_s = (3.68 \cdot 10^{-17} N Z^{1/2})^{-1}, \quad (2)$$

which varies according to the number of atoms per unit volume (N) and the atomic number (Z).

The signal measured by the SEM (N_{SEM}) is proportional to the number of protons (N_p), related via a calibration factor (C_f):

$$C_f = \frac{N_p}{N_{SEM}}. \quad (3)$$

This calibration factor is linked to the SEY and other properties, such as the electronics gain. More detailed information on this can be found in [6].

There are over 100 SEM monitors in the SPS complex, with varying *filling factors*, used for measuring different beam properties,: *single foils* (labelled as BSI) for beam intensity; *split foils* (BSP or BSM) for beam position; and *scanning single bands* (BBS) or *multiple band grids* (BSG) for both beam position and size. All of them are equipped with the same Data Acquisition System (DAQ), publishing the spill signals every 20 ms.

Given the nature of SE processes, like the SEY dependence on material properties (e.g. oxidation, vacuum conditioning, radiation damage, etc...) and the low particle fluxes to be

monitored, absolute calibration and signal to noise are very challenging to control and optimize.

BEAM INTENSITY STUDIES

The SEY variation over time is particularly relevant for the BSI monitors, providing the experiments with accurate Proton On Target (POT) values.

Most of the SEMs in the TT20 area were installed in the late 1970s [7] and only refurbished when highly damaged. The presently used calibration factor, mainly composed by the SEY and the DAQ gain, is the result of dedicated studies in the 1990s [6].

Re-evaluation of the BSI absolute calibration was re-started in 2016. Due to the low extracted DC beam current in the slow extracted beam lines, determining the absolute calibration is not straightforward. Direct calibration with a BCT in the line during a fast extraction, as done in the CERN Proton Synchrotron (PS) to East Area beam line, is not currently possible at the SPS and there are no plans to implement it for the foreseeable future.

Figure 2 shows intensity measurements taken in 2017 by 2 BSI foils located inside the same tank in the TT20 beamline, correlated to the Beam Current Transformer (BCT) measurement in the SPS ring before de-bunching and extraction.

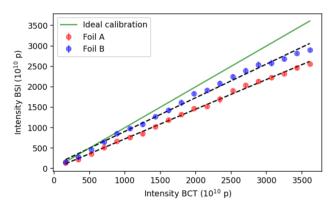We would expect to see a linear relationship between BSI

Figure 2: Intensity measured by BSI foils as a function of the intensity measured by BCT 2017.

and BCT, with slope equal to 1, in the ideal case of lossless extraction and perfect BSI calibration[2]. Non linearity could arise from SEY drift in time, DAQ dependence on signal level, or variation of losses with beam intensity.

A slope deviating from 1 could indicate systematic errors in the BSI calibration (e.g. SEY and DAQ gain), or the value for absolute extraction losses, which cannot be inferred by evaluating BCT and BSI values alone.

We also see non-linearity in Fig. 3, which shows how the ratio of intensities measured by the BSI[3] and BCT evolve over time. Interestingly the similarity in measurements between the two foils changes over time.

---

[2] BCT calibration is expected to be better than 1%
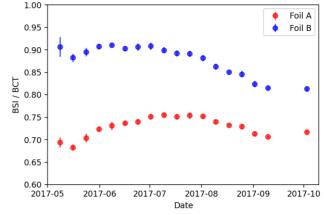[3] The intensity of the BSI foils was calculated using the latest calibration available.

Figure 3: Intensity measured by BSI foils normalised by intensity of BCT as a function of time.

Therefore the examples in the figures clearly show the uncertainty on the single foil calibration and the *cross-talk* between foils (downstream foil also measures SE from charged particles generated by the first foil). These problems and other related issues are discussed in more detail in [7, 8].

A method for calibration, frequently used in the CERN Proton Synchroton (PS) experiment lines, is the activation method, described in [6, 9]. This method relies on measuring ^{24}Na activity of a thin foil (e.g. in Aluminum), exposed to the beam, located as close as possible to the BSI to be calibrated.

After exposure for a certain period of time, the foil is removed from the beamlines and the activation measured using a gamma spectrometer. From the activation one can infer the integrated number of protons that traversed the foil. This can be used to calibrate the BSI, by comparing the activation measured in the foil to the counts measured by the BSI during the exposure period. With this method the calibration accuracy is dominated by the error on the activation process cross section, normally known within 10%.

This method, although previously shown to be effective, is disruptive to beam operation: it requires stops to insert and remove the devices from the beamline, so needs to be planned in advance.

Despite this disadvantage, it is one of the only reliable options for determining the absolute calibration in the TT20 beamline and will be used in future calibration studies. In addition to this Montecarlo simulations of beam interactions with SEM monitors will be conducted, using Geant4, to investigate both the absolute calibration and changes to SEM monitor design. These simulations are currently under development.

MACHINE LEARNING STUDIES FOR BEAM PROFILE AND POSITION

BBSs (single bands that move to scan the beam) and BSGs (horizontal or vertical bands, normally 16 per plane, each

connected to a separate DAQ channel) are used for beam position and profile measurements.

Each band intercepts only a part of the total beam measured by the BSIs. In this case absolute calibration is no longer relevant, since it is still possible to measure the position and profile without precise knowledge of the absolute number of protons. The challenge is to distinguish the background generated by different particles from sources of electronic noise, and therefore maximise the signal to noise ratio.

Traditionally signal processing can be used to reduce the noise, but more recently there have been some applications that have used machine learning techniques for this purpose [10]. In this contribution we explore the possibility of reducing the noise in the signals of the BSGs using *autoencoders*.

An autoencoder is a deep neural network commonly used for image processing. As depicted in Fig. 4, it consists of two basic sections, the first part compresses the original image into a lower dimensional representation, via a series of layers. The second part mirrors the original layered structure, taking the compressed representation (also referred to as latent space) and trying to reconstruct the original image. Some resolution can be lost in this process. We aim to
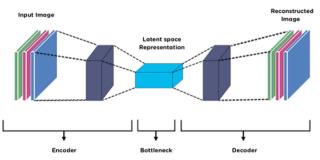

Figure 4: Graphic representation of Autoencoder sourced from [11].

exploit this resolution loss to our advantage: by creating a latent representation that is low enough, to create a smoothing effect, yet still able to retain the important features, needed for beam position and profile measurements.

To test this application a combination of TensorFlow [12] and Keras [13] libraries were used to implement the following autoencoder architecture: encoder containing one 2D convolutional layer, one 2D max pooling layer; decoder: containing one 2D upsampling layer, one 2D convolutional layer.

The data that was fed to the autoencoder, consisted of a matrix containing the signal of each channel, corresponding to a wire of a BSG. The matrix was of dimensions 264×16. 264 corresponding to the number of data points in time in the spill (one every 20 ms) and 16 corresponding to the number of channels in the BSG.

This data was then pre-processed before being passed to the autoencoder. The pre-processing involved two steps: first of all adding padding to change the matrix dimensions from
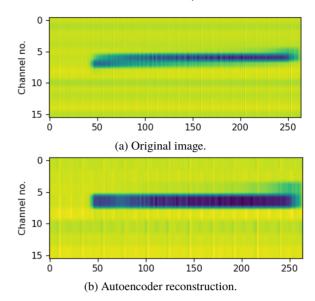

(a) Original image.

(b) Autoencoder reconstruction.

Figure 5: Example of autoencoder reconstruction.

264×16 to 264×264, then scaling all the data points by subtracting the mean and dividing by the standard deviation. The pre-processed data for one BSG device was split into training and testing samples. 3117 training samples were then used to train the autoencoder. The training was carried out over 19 epochs, using a batch size of 240, the Adam optimiser, with a learning rate of 0.6×10^{-3} and the loss function was Binary Crossentropy.

Results

The trained model was first used to reconstruct the test data for the same BSG device (labeled as BSGH.211706). Subsequently the trained model was fed with data from 5 other BSG devices. Figure 5 pictures the original and the reconstructed image, with data samples from BSGV.210156. Comparing the original and the reconstructed image we can see that the profile is a bit broader in the reconstructed image and that it is overall a bit smoother.

Figure 6 shows the signal integral over all BSG channels as a function of time in the spill, for the original data and the data reconstructed by the autoencoder. In the original data set the larger error bars suggest a wider spread of data (ie:noise). The reconstructed data set, has smaller error bars, thus evidencing a reduction in the noise.

A plot to show the comparison of the effects of the autoencoder on the profile of the beam at a fixed point in time was also made (Fig. 7). Here we see a broadening of the profile peak in the reconstructed image, but also a smoother image, with noise reduced at the tails. This is beneficial in most of the operational cases, where beam position and size are inferred from the distribution mean and standard deviation.

Overall, the results obtained from the autoencoder reconstruction across the other BSGs, were similar to those presented in this paper, although there was some variation, depending on the instrument and the point in time where the profile was taken. It would be interesting to further in-
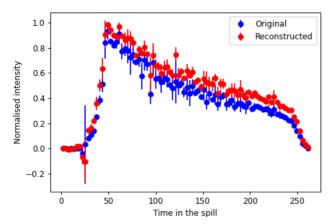
Figure 6: Comparison of normalised intensity as a function of time in the spill.
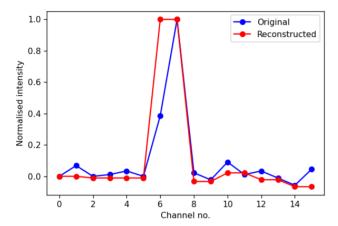

Figure 7: Comparison of normalised intensity as a function of channel number.

vestigate and quantify these variations and to include more devices in the analysis.

These initial results in noise reduction seem promising and could help improve the steering of the beam in the future, but still need to be validated for a conclusive evaluation.

CONCLUSION

Renewed interest in the fixed target experimental areas, has brought to attention the problems related to ageing SEM instrumentation present in these areas. This instrumentation requires upgrading and calibration in order to meet the needs of operators. In this contribution we have outlined the main challenges regarding these instruments, presenting the path currently being taken to solve these issues.

The first of these challenges is the absolute calibration of the BSI monitors in the TT20 beamline, which is limited by the absence of BCTs in the beamline. We are currently developing simulations to better understand the interaction between the beam and the instruments and we have plans to use the activation method as part of our absolute calibration studies.

The second major challenge affecting the profile and position measuring devices is the signal to noise ratio. In this

contribution we have explored the use of autoencoders for noise reduction, presenting preliminary results. An autoencoder was trained on the data of one BSG device and the trained model was then tested on the data of 5 other devices.

The autoencoder was able to reconstruct the data successfully, reducing the noise, but also increasing the width of the profile. Not all results were consistent and in future we aim to quantify how consistently the autoencoder performs across different devices. We also aim to compare the modified signal, with a reference signal for a more complete validation.

ACKNOWLEDGEMENTS

REFERENCES

[1] M. A. Fraser *et al.*, "Slow Extraction Efficiency Measurements at the CERN SPS," in *Proc. IPAC'18*, Vancouver, Canada, Apr.-May 2018, pp. 834–837. `doi:10.18429/JACoW-IPAC2018-TUPAF054`

[2] J. Wenninger, *SPS operation,* `https://jwenning.web.cern.ch/SPS.html`

[3] A. N. Fernandez, D. Belohrad, C. Bracco, E. Renner, F. Roncarolo, and J. Tassan-Viol, "PSB H0-H- Monitor Calibration and Commissioning," in *Proc. IBIC'21*, Pohang, Korea, Sep. 2021, p. 429. `doi:10.18429/JACoW-IBIC2021-WEPP24`

[4] E. J. Sternglass, "Theory of secondary electron emission by high-speed ions," *Phys. Rev.*, vol. 108, pp. 1–12, 1957. `doi:10.1103/PhysRev.108.1`

[5] D. Kramer, "Design and Implementation of a Detector for High Flux Mixed Radiation Fields," Ph.D. dissertation, Technical University of Liberec, Czechia, 2008. `http://cds.cern.ch/record/1139227`

[6] K. Bernier *et al.*, "Calibration of secondary emission monitors of absolute proton beam intensity in the CERN SPS North Area," CERN, Geneva, Switzerland, Tech. Rep., 1997. `doi:10.5170/CERN-1997-007`

[7] I. Ortega *et al.*, *North area beam instrumentation consolidation type: Na-cons groups: Be-bi & en-ea*, EDMS no. 2141518. `https://indico.cern.ch/event/826747/ contributions/3458702/attachments/1873506/ 3087270/NACONS_Request-BE-BI-V2.1.pdf`

[8] M. Fraser and F. Velotti, *Upgraded beam instrumentation for slow extraction at sps*, EDMS no.2113420. `https: //indico.cern.ch/event/807016/contributions/ 3359176/attachments/1816894/2969841/FS-BI- SLAWG_-_2113420_v0.1.pdf`

[9] A. Chapman-Hatchett *et al.*, "Calibration of the secondary emission monitors TBIU and TBID of the North Area targets stations T2, T4, and T6 in TCC2 for slow extracted protons of 400 GeV," CERN, Geneva, Switzerland, Tech. Rep., 1979. `https://cds.cern.ch/record/2816600`

[10] E. Almazrouei, G. Gianini, C. Mio, N. Almoosa, and E. Damiani, "Using autoencoders for radio signal denoising," in *Proc. 15th ACM Symposium on QoS and Security for Wireless and Mobile Networks*, 2019, pp. 11–17. `doi:10.1145/3345837.3355949`

[11] D. Birla, *Basics of autoencoders*, 2019, `https://medium.com/@birla.deepak26/autoencoders-76bb49ae6a8f`

[12] M. Abadi *et al.*, *TensorFlow: Large-scale machine learning on heterogeneous systems*, 2015, `https://www.tensorflow.org`

[13] F. Chollet *et al.*, *Keras*, 2015, `https://keras.io`